5th International Conference on Experimental Fluid Mechanics ICEFM 2018 Munich
Munich, Germany, July 2-4, 2018

The Influence of Boundary-Layer Turbulence on Gust-Response Transfer Functions

Nathaniel Wei[1*], Johannes Kissing[1], Tom Wester[2], Klaus Schiffmann[1], Cameron Tropea[1]

[1] Technische Universität Darmstadt, Institute of Fluid Mechanics and Aerodynamics, Darmstadt, Germany

[2] University of Oldenburg, ForWind, Institute of Physics, Oldenburg, Germany

[*]njwei@stanford.edu

Abstract

The Sears function models the unsteady lift force on an airfoil in a sinusoidal gust using potential flow arguments. However, Jancauskas and Melbourne (1983) hypothesized that increasing turbulence intensity would improve, rather than detract from correspondence with the Sears function. In order to test this hypothesis, a sinusoidal-gust generator was used to evaluate the gust response of a NACA 0006 airfoil in highly laminar inflow conditions, with reduced frequencies between 0.095 and 0.64 and Reynolds numbers from 130,000 to 330,000. A strip of tripping tape induced a turbulent boundary layer on the airfoil's surface. The gust-response data from the airfoil with tripping tape converged to the Sears function significantly better than those from the unmodified airfoil. This suggests that the turbulent boundary layer causes the flow to remain attached to the airfoil, so that flow separation is avoided and the assumptions of Sears' theory are better satisfied. These results imply that the Sears function could also be applied to airfoils with turbulent boundary layers, thereby increasing its range of use.

1 Introduction

Despite nearly one hundred years of scrutiny, the fundamental problem of an airfoil encountering a gust has remained highly relevant to modern aerodynamics. Gust-airfoil interactions affect animal flight, helicopter rotors, fixed-wing aircraft, and wind turbines, and in engineering design it is imperative that wind gusts do not bring large load fluctuations to bear on critical structures. To predict the effects of gusts on the loading of a wing, Sears (1938) developed a first-order transfer function for a thin airfoil encountering a sinusoidal gust. This transfer function relates the dynamic lift induced by a gust with a certain gust-angle amplitude $\hat{\alpha}_G$ to the lift generated across the same angle-of-attack amplitude in quasi-steady flow:

$$h_L = \hat{h}_L e^{-i\phi} = \frac{\hat{L}_{dyn}}{\hat{L}_{qs}} e^{-i(\phi_{dyn}-\phi_{qs})}, \tag{1}$$

where the subscripts *dyn* and *qs* denote dynamic and quasi-steady quantities. h_L is only a function of the reduced frequency k, defined as $k = \pi \frac{fc}{U_\infty}$, where c is the length of the airfoil chord and f is the gust frequency in Hz, as given in Leishman (2006). Application of the model requires that the assumptions of thin-airfoil theory hold, and that the gust disturbances remain small. An important characteristic of the transfer function is that it decreases monotonically from a value of unity at $k = 0$, suggesting that at no reduced frequency will the fluctuating loads be amplified above their quasi-steady values. The theory has been extended by Goldstein and Atassi (1976) and Lysak et al. (2013), among others, to cover more complex flow conditions.

Because of the general applicability of the gust-interaction problem, a number of studies have attempted to determine the validity of the Sears function under experimental conditions. The majority of these (e.g. Sankaran and Jancauskas (1992), Larose (1999), and Hatanaka and Tanaka (2002)) used velocity and force spectra to extract a range of reduced frequencies from a single turbulent inflow condition. Studies using a thin airfoil showed general agreement with Sears' theory, while studies with a cross-section of a bridge deck showed significant deviation from theoretical predictions.

In contrast, relatively few studies have attempted to model the actual flow condition imposed by Sears: sinusoidal velocity oscillations normal to the profile. Most of these were inconclusive, with the notable exception being the work of Jancauskas and Melbourne (1983). They produced well-characterized sinusoidal gusts up to a reduced frequency of $k = 0.33$ using a pair of controlled-circulation airfoils, and gust-response measurements on a NACA 0006 airfoil demonstrated a near-perfect correspondence with the Sears function. The authors also observed a significant deviation from the theory that remarkably decreased with increased turbulence intensities when testing the cross-section of a bridge deck. They thus hypothesized that introducing turbulence into the free-stream flow delayed separation from the airfoil, thereby maintaining the Sears inflow conditions more closely. This hypothesis is intriguing because it suggests that the nominally laminar theory of Sears performs better under turbulent gust conditions, which are also found far more frequently in applications than laminar flows with gusts.

This study aims to test this hypothesis directly. The assumption that turbulence facilitates flow attachment implies that the boundary layer is somehow affected by the turbulent inflow conditions. Therefore, in these experiments, the boundary layer itself is directly influenced, and the gust conditions are controlled to match the assumptions of Sears as closely as possible. A fully two-dimensional active grid is used to project sinusoidal gusts onto a NACA 0006 airfoil, and a thin strip of tripping tape just behind the leading edge of the airfoil is used to induce transition in the nominally laminar boundary layer. The sinusoidal gusts are characterized using two-component hot-wire probes, and two-camera stereoscopic particle image velocimetry (stereo PIV) allows flow separation to be identified. Through this procedure, the effects of boundary-layer turbulence on the Sears function are experimentally quantified, and the hypothesis of Jancauskas and Melbourne can thus be generalized to lifting profiles with turbulent boundary layers.

2 Experimental Setup

The experiments reported in this study were carried out in a closed-loop wind tunnel at the University of Oldenburg (cf. Knebel et al. (2011)). The test section had a cross-sectional profile of 1.00×0.80 m^2. An active grid was installed in the tunnel at the front of the test section, 1.1 m upstream from the quarter-chord point of the airfoil. It was composed of six 3D-printed paddles, each with a NACA 0016 cross-sectional profile with 78 mm chord and 0.8 m span. The paddles were installed on the left and right sides of the grid, which kept the wakes of the paddles from influencing the test airfoil. The turbulence intensity in the middle of the tunnel, computed from hot-wire data, was less than 0.3%. The paddles were pitched about their quarter-chord point in sinusoidal profiles with a given amplitude and frequency, though the paddles near the walls were prevented from rotating toward the walls in order to avoid reflecting gusts off the walls. A diagram of the wind tunnel and active grid is shown in Figure 1.

The active grid was characterized using two-component hot-wire anemometry probes. The amplitude of the angle-of-attack fluctuations produced by the grid, denoted by $\hat{\alpha}_G$, was measured across a large range of free-stream velocities, grid frequencies, and grid paddle amplitudes. A power-law fit was applied to the gust-angle amplitude ($\hat{\alpha}_G$) versus grid paddle amplitude ($\hat{\theta}$) data for each combination of frequency and free-stream velocity. These fits allowed the grid paddle amplitude to be selected in order to produce a desired gust-angle amplitude for a given reduced frequency. In this manner, the gust-angle amplitude could be precisely controlled.

The flow conditions were additionally quantified with a LaVision stereo PIV system, composed of two Phantom Miro M320S high-speed cameras, each with a maximum recording duration of approximately 5 seconds, mounted above and below the test section. A Litron LDY-303 Nd:YLF dual-cavity high-speed pulsed laser illuminated the suction side of the airfoil from the rear of the tunnel. Images were recorded with LaVision's DaVis software at a rate of 500 Hz. The images were correlated using the software PIVview3C from PIVTEC Gmbh with 16×16-pixel interrogation areas, 50% overlap, and outlier interpolation.

To serve as the test profile, a NACA 0006 airfoil with a 202 mm chord and 800 mm span was constructed at the TU Darmstadt. It was composed of two carbon-fiber shells attached to an aluminum spine, so that the airfoil was both smooth and rigid against torsion. This profile was selected to conform to the thin-airfoil assumption of Sears and to serve as a comparison with the experiments of Jancauskas and Melbourne. A thin strip of fluorescent foil at the location of the laser sheet reduced surface reflections.

A pair of K3D120 3-axis force balances and a TS110 moment sensor from ME-Messsysteme allowed forces and moments to be measured at the airfoil's quarter-chord point. 30 seconds of force data were collected for each measurement. Stereo PIV and force measurements were started simultaneously via a trigger provided two seconds after the active-grid protocol was started.

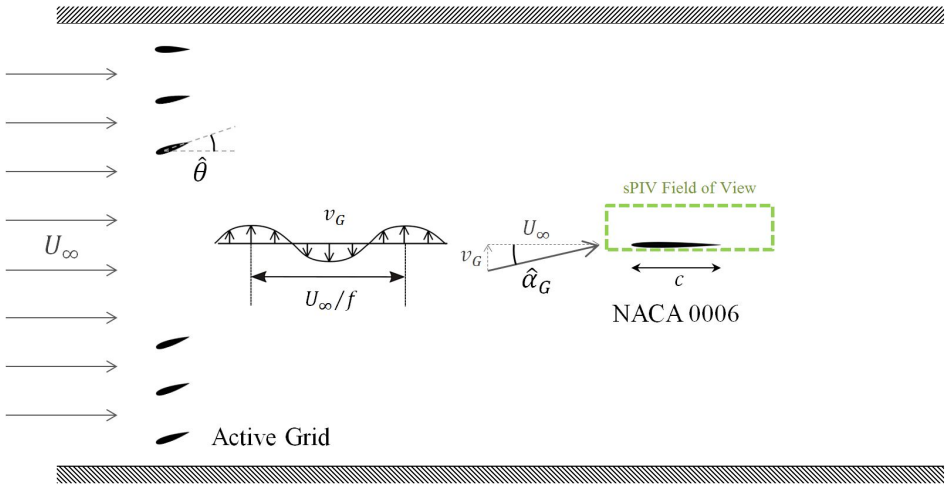

Figure 1: Top view of the Oldenburg active-grid wind tunnel, showing active grid in motion (with the top two paddles limited in amplitude to avoid directing flow into the walls), NACA 0006 airfoil, and approximate location of the stereo PIV field of view.

3 Design of Experiments

In order to produce the Sears function, a range of active-grid frequencies and free-stream velocities was selected. The airfoil was held at an angle of attack of $\alpha_m = 0^\circ$. A fixed gust-angle amplitude of $\hat{\alpha}_G = 2^\circ$ was chosen in order to avoid flow separation on the thin airfoil, as predicted in the steady case by XFOIL. This choice of $\hat{\alpha}_G$ also maintained a significant signal-to-noise ratio over a wide reduced frequency range. The active-grid paddle amplitudes $\hat{\theta}$ were set based on the hot-wire data fits to maintain this value of $\hat{\alpha}_G$. Velocities of $U_\infty = 10$, 15, 20, and 25 m/s were combined with frequencies between 4 and 10 Hz to obtain a reduced frequency range from $k = 0.095$ to $k = 0.64$. Out of the 18 reduced frequencies shown in this study, six critical cases were selected for analysis with stereo PIV.

The row of 18 distinct measurements were carried out on the unaltered NACA 0006 airfoil and the same airfoil with two thin strips of tripping tape, 3.5 mm in width and 0.1 mm thick, laid directly behind the leading edge of the airfoil on either side at around $x/c = 0.05$.

To compute transfer function values from experimental data, the force data were first shifted from the airfoil frame of reference to that of the wind tunnel. The first two seconds of each data set were discarded in order to remove start-up effects. A Fourier transform of the signal yielded the magnitude of the lift force fluctuations, corresponding to $\hat{L}_{dyn}$ from Equation 1. The quasi-steady lift amplitude $\hat{L}_{qs}$ was interpolated from steady lift curves L_{U_∞} using the relation

$$\hat{L}_{qs} = f(U_\infty, \hat{\alpha}_G, \alpha_m) = \frac{1}{2}\left(L_{U_\infty}(\alpha_m + \hat{\alpha}_G) - L_{U_\infty}(\alpha_m - \hat{\alpha}_G)\right). \tag{2}$$

The data points were validated using both force-balance data and, for the six cases in which stereo PIV was employed, phase-averaged velocity vector fields. Error bars were computed from the standard deviation of the phase-averaged lift-force signal and the standard deviation of the gust-angle amplitudes from hot-wire data. For data taken at $U_\infty = 10$ m/s, no hot-wire data was available, and therefore gust-angle amplitudes were extracted from the stereo PIV vector fields and errors were estimated.

It was expected that the Fourier transformed lift-force data would show a single large peak at the frequency of gust generation, but occasionally smaller peaks at other frequencies were observed. If any of these secondary peaks were over 20% as large as the main peak, this suggested that the lift force was not purely sinusoidal. These data sets were then removed from the transfer function plot, so that the resulting data only represented single frequency sinusoidal gusts. One such phase-averaged lift-force signal and corresponding Fourier transform is shown in Figure 2(a).

A criterion for flow separation was developed using the fact that turbulent flows have much stronger three-dimensional character than laminar flows. Each stereo PIV vector field was thus divided in half diagonally, as shown in Figure 3, so that the airfoil and its wake region lay in one section and the other section

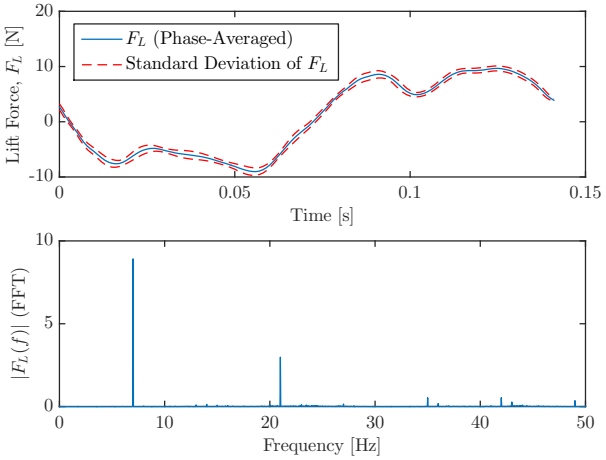

(a) Phase-averaged lift force signal for a 7-Hz gust at $U_\infty = 25$ m/s, with a problematic secondary peak at 21 Hz.

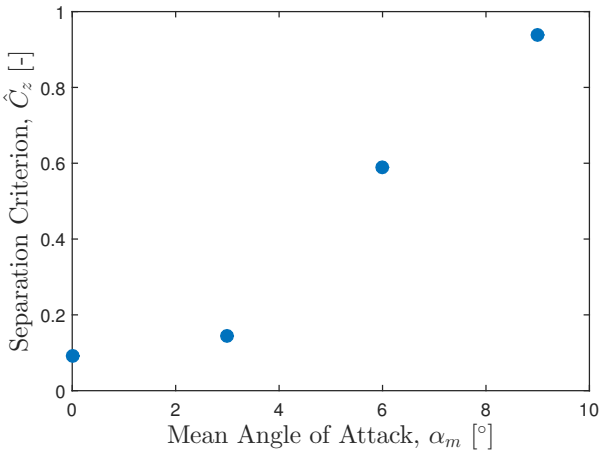

(b) Separation criterion values for a 6-Hz gust at $U_\infty = 20$ m/s and a range of airfoil angles of attack.

Figure 2: Validation criteria for experiments, based on (a) force spectrum data and (b) stereo-PIV data.

contained nominally undisturbed flow. The magnitude of the spanwise velocity component $|v_z|$ was averaged across each region, and the ratio of these values was taken for each vector field as $C_z(t) = \overline{|v_z|_{foil}}/\overline{|v_z|_{flow}}$. Finally, the amplitude of this quantity was computed over a single phase-averaged period, yielding the separation criterion $\hat{C}_z$.

The parameter $\hat{C}_z$ thus provides a comparison between spanwise velocity components near the airfoil and in the free stream, and thereby can be used to quantify the relative presence of separation in a given stereo PIV image pair. For laminar flows, $\hat{C}_z \approx 0$. The values of this criterion are shown for gusts with amplitude $\hat{\alpha}_G = 1.24°$ are shown in Figure 2(b) for a range of mean angles of attack. For these cases, the separation criterion reflected the anticipated amounts of separation quite well. For the cases with zero mean angle of attack, however, it was not sensitive enough in its current implementation to distinguish between cases. This criterion was therefore not used to remove data from the transfer function plots. However, its accurate characterization of unsteady separation across a range of mean angles of attack suggests that the criterion could perform well for airfoils with zero mean angle of attack if the velocity vector fields are filtered to remove noise.

4 Results and Discussion

The measured values for the magnitude of the transfer function on the unmodified airfoil and the airfoil with tripping tape are shown in Figures 4(a) and 4(b) respectively. The R^2 value, a measure of the goodness of fit between the data and theoretical prediction, is significantly higher for the data recorded with tripping tape than for those recorded on the unmodified airfoil ($R^2 = 0.737$ vs. $R^2 = 0.475$), showing that the spread of the data is greatly reduced in the presence of tripping tape. The data points taken at $U_\infty = 10$ m/s consistently fall below the Sears curve. The gust-angle amplitudes for these cases, however, were not validated with hot-wire measurements. The slight upward trend visible at $U_\infty = 15$ m/s and the high values at $U_\infty = 25$ m/s are most likely due to the onset of flow separation and dynamic effects. In order to verify this conjecture, the separation criterion discussed previously will need to be tuned to detect smaller separation regions close to the airfoil's surface.

The turbulence intensity of the Oldenburg wind tunnel was significantly smaller than that of Jancauskas and Melbourne's experiment ($< 0.3\%$ vs. 0.6%). Their hypothesis that increased turbulence intensity leads to better correspondence with the Sears function makes sense of the fact that their data converge more cleanly than those presented in this study.

The demonstrated influence of the presence of tripping tape further confirms this hypothesis. With a turbulent flow field produced by a passive grid and disturbed by sinusoidal gusts, as in the experiments of Jancauskas and Melbourne, it is harder to say exactly what effect the background turbulence has on the

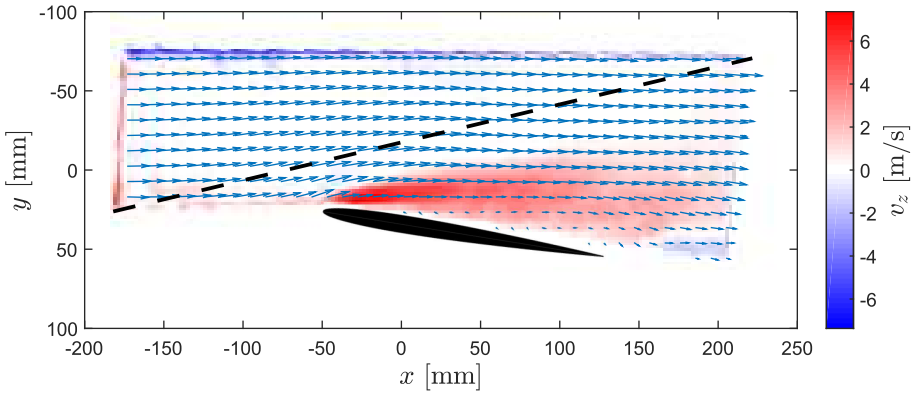

Figure 3: Stereo PIV vector field, with dashed black line indicating the division of regions for calculating the separation criterion $\hat{C}_z$, for a 10-Hz gust with $\hat{\alpha}_G = 2^\circ$ and $U_\infty = 15$ m/s. $\alpha_m = 9^\circ$, the highest investigated, is displayed to show that the upper region is representative of the free stream in all cases.

airfoil. In contrast, this study induced transition to turbulence on the airfoil's surface itself. Since a turbulent boundary layer stays attached longer to a surface than a laminar boundary layer, the turbulent flow on the airfoil with tripping tape will follow the profile more closely, and therefore more closely match the potential-flow conditions imposed by Sears' theory. It can thus be inferred that the turbulent boundary layer present on the airfoil is directly responsible for the better convergence of the data to the Sears function.

The purpose of this study is not to determine the physical difference between turbulent gusts on an airfoil and nominally laminar gusts on an airfoil with a turbulent boundary layer. Rather, the experiments show that the effects of these two flow conditions are similar in terms of their effect on gust-response data. In addition to the flow-attachment argument put forth by Jancauskas and Melbourne, it is possible that the impulse from gust to airfoil is better transmitted under turbulent conditions. Further experiments are required to obtain a better understanding of the flow physics at work in this problem.

5 Conclusion

This study sought to verify the Sears function on a NACA 0006 airfoil, and test the hypothesis that introducing a turbulent boundary layer could improve experimental convergence with theoretical predictions. Inducing turbulent transition using tripping tape near the airfoil's leading edge showed that the turbulent boundary layer does indeed shape the flow conditions to conform to Sears' assumptions, thereby leading to better agreement with the theory despite clear violation of potential-flow theory assumptions.

Further work on the separation criterion introduced in this paper will allow the effects of turbulence on flow separation and dynamic stall to be more precisely investigated. More comprehensive measurements of the flow on the surface of the airfoil using an infrared camera would enable the fluid dynamics of the boundary layer itself and its interactions with the oncoming gusts to be quantified and analyzed. Lastly, the current experimental apparatus allows other models for unsteady aerodynamics, such as those of Atassi and Lysak, to be validated and explored.

The finding that a turbulent boundary layer can increase correspondence with the Sears function has implications for the theory's applicability to real-world situations. A turbulent boundary layer exists naturally on many airfoils because of their shape and surface roughness. The results presented here suggest that, though these airfoils may not fulfill the requirements of potential-flow theory, the Sears function may nevertheless represent their gust-response characteristics quite well. Since most gust-loading applications involve turbulent flow, the Sears function may be applicable in practice to a much larger range of situations than its assumptions would imply.

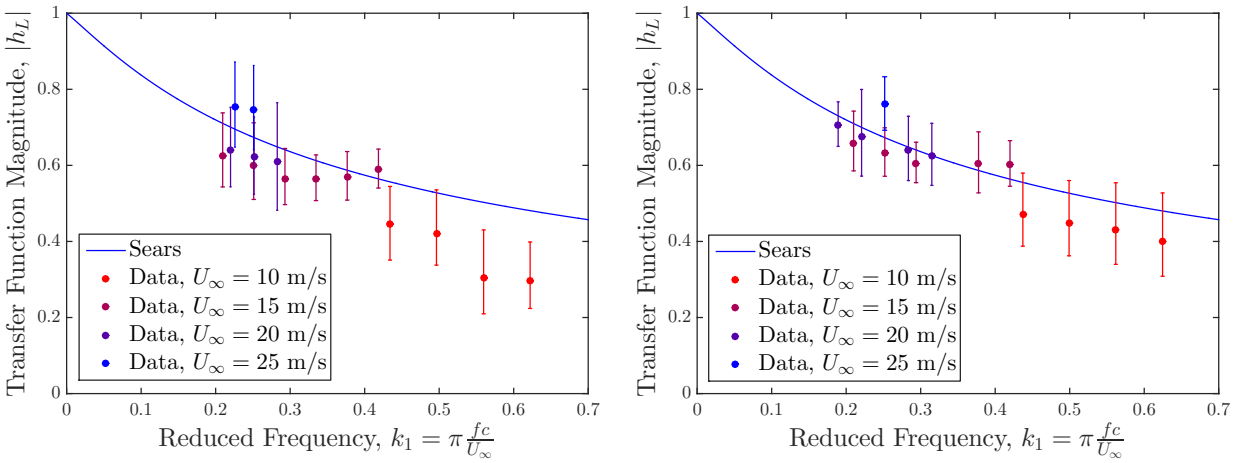

(a) Experimental data from the unmodified NACA 0006 airfoil; $R^2 = 0.475$.

(b) Experimental data from the NACA 0006 airfoil with tripping tape; $R^2 = 0.737$.

Figure 4: Experimental data for the Sears transfer function, organized by free-stream velocity, for (a) the unmodified NACA airfoil and (b) the airfoil with tripping tape.

Acknowledgements

Funding for these investigations was graciously provided by the German Research Foundation (DFG) CDZ project #317970247 and the DFG PAK 780 project. The work of Nathan Wei was supported by a student research grant from the Fulbright U.S. Student Program and the German-American Fulbright Commission.

References

Goldstein ME and Atassi H (1976) A complete second-order theory for the unsteady flow about an airfoil due to a periodic gust. *Journal of Fluid Mechanics* 74:741–765

Hatanaka A and Tanaka H (2002) New estimation method of aerodynamic admittance function. *Journal of Wind Engineering and Industrial Aerodynamics* 90:2073–2086

Jancauskas ED and Melbourne WH (1983) The Aerodynamic Admittance of a Slender Box Girder Bridge Section. Newcastle, Australia

Knebel P, Kittel A, and Peinke J (2011) Atmospheric wind field conditions generated by active grids. *Experiments in Fluids* 51:471–481

Larose GL (1999) Experimental Determination of the Aerodynamic Admittance of a Bridge Deck Segment. *Journal of Fluids and Structures* 13:1029–1040

Leishman GJ (2006) *Principles of Helicopter Aerodynamics*. Cambridge University Press, New York. 2nd edition

Lysak PD, Capone DE, and Jonson ML (2013) Prediction of high frequency gust response with airfoil thickness effects. *Journal of Fluids and Structures* 39:258–274

Sankaran R and Jancauskas ED (1992) Direct measurement of the aerodynamic admittance of two-dimensional rectangular cylinders in smooth and turbulent flows. *Journal of Wind Engineering and Industrial Aerodynamics* 41:601–611

Sears WR (1938) *A systematic presentation of the theory of thin airfoils in non-uniform motion*. Ph.D. Dissertation. California Institute of Technology